

Synthesis of Octabromoperylene Dianhydride and Diimides: Evidence of Halogen Bonding and Semiconducting Properties

Yogendra Kumar,[†] Sharvan Kumar,[†] Sudhir Kumar Keshri,[†] Jyoti Shukla,[†] Shiv Shankar Singh,[‡] Tejender S. Thakur,[‡] Mitchell Denti,[§] Antonio Facchetti,^{*,§,||} and Pritam Mukhopadhyay^{*,†}

[†]Supramolecular and Material Chemistry Lab, School of Physical Sciences, Jawaharlal Nehru University, New Delhi 110067, India

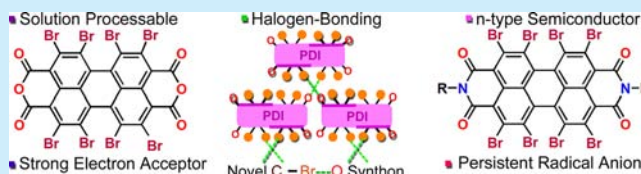
[‡]Molecular and Structural Biology Division, CSIR- CDRI, Lucknow 226031, India

[§]Polyera Corporation, Skokie, Illinois 60077, United States

^{||}Department of Chemistry, Northwestern University, Evanston, Illinois 60208, United States

S Supporting Information

ABSTRACT: A facile synthesis of octabromoperylene-3,4,9,10-tetracarboxylic dianhydride (Br₈-PDA) (**1**), its diimides (Br₈-PDI) (**2a–e**), and bis-, tris-, and tetra-amino substituted diimides (**5a–c**) with six, five, and four remaining substitutable Br atoms, respectively, is reported. Octabromination results in facile chemical/electrochemical reduction, radical anion formation, and red-shifted optical properties. For the first time, diverse halogen-bonding interactions were identified in the PDA/PDI, which along with the attractive electronic features enhance the electron-transport characteristics compared to the di-/tetra-brominated PDIs (**3/4**).



Perylenediimides (PDIs) have attracted growing interest for their unique self-assembly, optoelectronic properties, and use as novel semiconductors.^{1–3} Halogenation of PDIs offers a great platform to tune these properties and to explore new reactions.^{4,5} New strategies have been developed to obtain high yields of multihalogenated PDIs at the bay positions, e.g., the recent access to pure tetra-chloro PDI.⁶ On the other hand, halogenation at the nonbay positions of PDIs has been scarcely studied, and full characterization is limited to octa-chloro-PDIs and a few other derivatives.⁷ Although a patent briefly reports on the octabromo-substituted perylene tetracarboxylic acid dianhydride (Br₈-PDA) and its diimidized derivatives, no spectroscopic data, physical characteristics, or structural information was disclosed for these compounds.⁸

There is a significant 26% volume increase moving from Cl (18.1 Å³) to Br (24.4 Å³). Therefore, electrophilic insertion of eight bromine atoms in the PDA scaffold poses steric as well as electronic challenges. Furthermore, bis-imidization of this bulky moiety with amines would be synthetically demanding. Finally, under the usual PDA imidization conditions, the even more reactive nonbay halogenated sites would be prone to ArS_N reactions. These issues may have deterred research toward octabromoperylene dianhydride and diimides.

On the other hand, we anticipated octabromination to drive new forms of self-assembly with the PDA/PDI scaffold due to the enhanced σ -hole effect.⁹ Notably, the halogen-bonding aspects have not been explored with the PDA/PDI scaffolds to date. The other advantage we envisaged is superior solubility due to the significantly reduced electronegativity differences of the C–Br vs C–Cl bonds and the increased polarizability of the Br atom. Overpassing the solubility constraints of the PDA

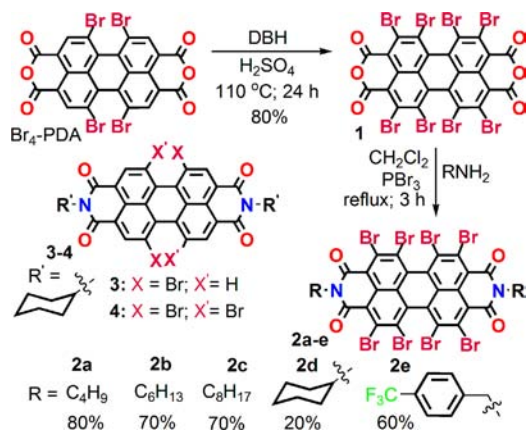
scaffold could enable us to characterize its optoelectronic properties in solution, unexplored to date.¹⁰ Finally, the prospect of widening the repertoire to include new PDI derivatives by controlling the ArS_N reactions and modulating acceptor/semiconductor properties motivated us to pursue this line of research.

Thus, in this study, we report the facile synthetic access to octabromoperylene-3,4,9,10-tetracarboxylic dianhydride (**1**), octabromoperylene-3,4,9,10-tetracarboxylic diimides (**2a–e**), and new donor–acceptor diimides (**5a–c**) and investigate their optical, electronic, and charge-transport characteristics. The study revealed new and diverse halogen-bonding motifs, hitherto unknown for the PDA and PDI scaffolds.

The reaction of Br₄-PDA^{4b} with 5,5-dimethyl-1,3-dibromohydantoin (DBH) in sulfuric acid at 110 °C resulted in the formation of Br₈-PDA (**1**) in good yields (Scheme 1). Notably, **1** was found to be soluble even in dichloromethane (0.20 mg/mL), chloroform (0.15 mg/mL), and tetrahydrofuran (5.00 mg/mL). The imidization of **1** could not be carried out by adopting conventional procedures, e.g., heating/refluxing the PDA with amines in propionic acid or *N*-methylpyrrolidinone.^{4–6} Aided by its solubility, we succeeded in the imidization of **1** in dichloromethane in the presence of phosphorus tribromide with a variety of alkyl-/benzylamines to produce **2a–e** with yields up to ~80% (Scheme 1). Noteworthy is that octabromo-PDI based on the patent requires ~4 days for its synthesis and uses the hazardous 30% oleum. In contrast, the present method is straightforward

Received: December 11, 2015

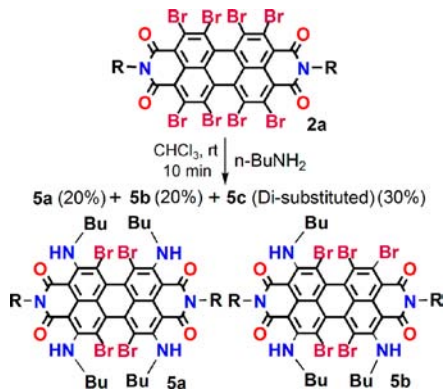
Published: January 15, 2016

Scheme 1. Synthesis of **1** and **2a–e**

and circumvents the use of the oleum. Finally, we also synthesized *N,N'*-dicyclohexyl-1,7-dibromoperylenebisimide (**3**) and *N,N'*-dicyclohexyl-1,6,7,12-tetrabromoperylenebisimide (**4**) as reference compounds to compare their optoelectronic characteristics to the new Br₈-PDIs. All of the compounds were characterized by conventional analytical techniques (see the [Supporting Information](#)).

Before studying in detail the comparative properties of **1–4**, we examined the potential to carry out controlled ArS_N reactions at the nonbay positions. Interestingly, by reacting **2a** with *n*-butylamine in chloroform at room temperature, three differentially substituted products (**5a–c**) were produced within 10 min of the reaction ([Scheme 2](#)). These products had a tunable number of amino donor groups, a variable number of substitutable Br atoms at the nonbay positions, and four Br atoms at the bay positions.

Scheme 2. Functionalization at Nonbay Positions



To understand the multibromination effect in the structure and packing features of the Br₈-PDA/Br₈-PDI scaffold, we sought X-ray crystallographic information. X-ray analysis¹¹ of **1** and **2a** revealed highly twisted perylene cores with a torsional angle (θ) of 40.1° and 38.8°, respectively, between the planes of rings BCF and DEG ([Figure 1a,b](#) and [Table S1](#)). These angles are close to that of Br₄-PDI ($\theta \sim 37.2^\circ$) but significantly larger compared to bay disubstituted Br₂-PDI ($\theta = 24.0^\circ$) and bay tetrasubstituted Cl₄-PDI ($\theta = 35.5^\circ$) derivatives.^{4a,12a} The Br atoms at the nonbay positions form intramolecular nonbonding Br \cdots O interactions with distances of 2.861 and 2.903 Å for **1** and 2.831 and 2.870 Å for **2a**, which is shorter than the sum of the van der Waals radii of Br and O atoms (3.35 Å).

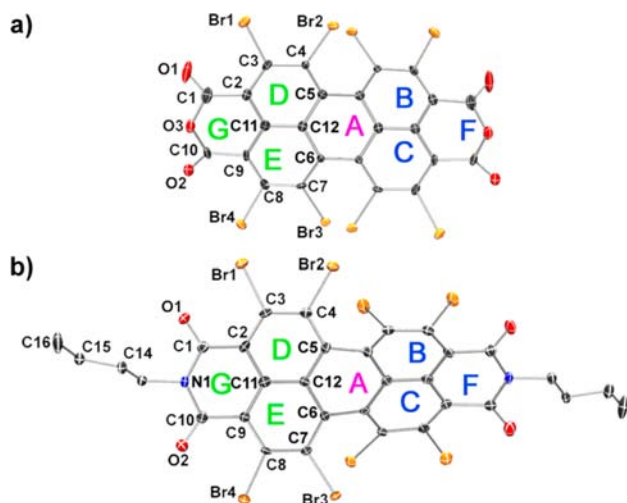


Figure 1. ORTEP drawing of the crystal structures of (a) **1** and (b) **2a** at 50% thermal ellipsoid probability. Both **1** and **2a** sit on a crystallographic 2-fold axis of symmetry.

Importantly, new and distinct self-assembly patterns were revealed for both the PDA and PDI scaffolds, hitherto unreported for these systems ([Figures S2–S4](#)). The self-assembly is driven by halogen bonding (XB) established by utilizing the σ -hole effect of Br as XB donor and the imide oxygen as the XB acceptor. In **1**, only the Br atoms at the nonbay positions participate in XB interactions ([Figure 2a](#))

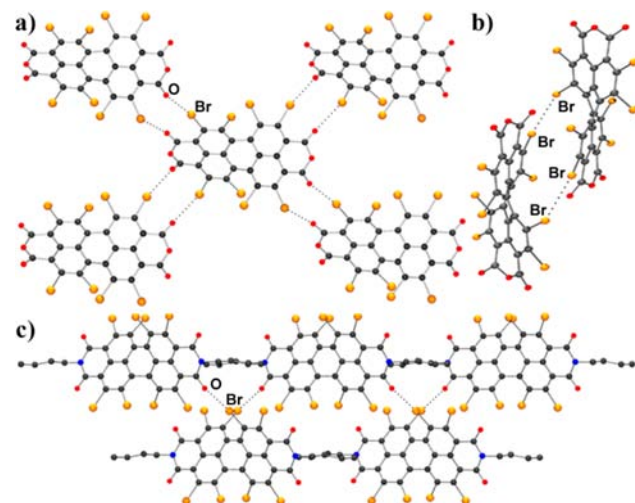


Figure 2. POV-Ray drawing showing different halogen bonding motifs: (a) Br \cdots O interactions of **1**, (b) Br \cdots Br interactions of **1**, and (c) Br \cdots O interactions of **2a**.

where each PDI unit forms four 10-membered cyclic XB assemblies with the neighboring PDIs. These 10-membered rings are constituted of two different C–Br \cdots O_(imide) interactions with Br \cdots O_(imide) distances ranging 2.94–3.22 Å and angles \angle C–Br \cdots O_(imide) of 167–122°. In addition, **1** exhibits type II XB interactions with Br \cdots Br distances of 3.445 Å and \angle C–Br \cdots Br' and \angle C–Br' \cdots Br angles of $\sim 161^\circ$ and 93° , respectively ([Figure 2b](#)). In sharp contrast, in **2a** only the Br atoms at the bay positions participate in XB interactions ([Figure 2c](#)). Criss-crossed and a slightly bent C–Br \cdots O_(imide)-type interactions were seen in the supramolecular array, with Br \cdots O_(imide) distances between 2.794 and 3.250 Å and \angle C–Br \cdots

O_(imide) angles of 130–174° (Figures S3 and S4). In addition, halogen $\cdots\pi$ interactions were found in **2a** with Br $\cdots\pi$ distances of 3.404 Å (Table S2). Notably, this type of Br $\cdots\pi$ halogen bonding was not found in any other halogen-substituted PDI systems.

Multiple-bromine functionalization in **1** provided adequate solubility in CH₂Cl₂ to measure the redox properties which, to the best of our knowledge, have not been quantified for PDAs due to solubility constraints. Cyclic voltammetry (CV) and differential pulse voltammetry (DPV) studies of **1** demonstrated two stepwise reversible electron reduction processes (Figure 3a,b). From the DPV measurements, the first and

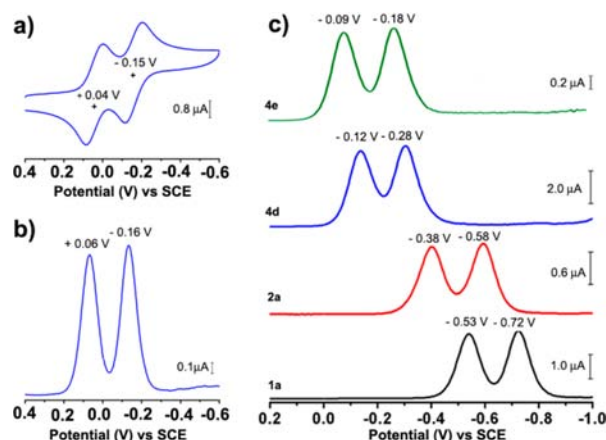


Figure 3. (a) CV and (b) DPV studies of **1**, (c) DPV of **2d**, **2e**, **3**, and **4** in degassed CH₂Cl₂; reference electrode, SCE; working and auxiliary electrode, Pt with 0.1 M Bu₄NPF₆; 298 K; scan rate, 200 mV/s (Supporting Information, Table S3A).

second reduction potentials of **1** are at +0.06 and −0.15 V versus SCE. From these data, we conclude the following: (a) the first and second reduction potentials in **1** are significantly shifted by \sim +590 mV and +560 mV, respectively, compared to the reference **3** molecule, (b) this dramatic positive shift of the reduction potential makes it one of the strongest air-stable PDA-based electron acceptors, and (c) a significant expansion of the electrochemical window to the positive direction opens up new possibilities of charge/electron transfer reactions with this air- and light-stable PDA scaffold.^{12a,c}

CV studies of **2a–e** confirmed a reversible stepwise two-electron reduction process (see the SI, Figure S1). The calculated HOMO–LUMO surfaces of **2a** are shown in Figure S5. In the case of the octabrominated PDIs, we observed that the acceptor groups at the axial positions, e.g., **2e** with a *p*-CF₃-benzyl group, can additionally shift the reduction potentials in the positive direction with respect to alkyl groups in **2d** (Figure 3c). Notably, a considerable degree of compression of the second reduction potential (ΔE) was also found in these systems, e.g., 90 mV for **2e** compared to 200 mV for **3** and 190 mV for **4**. In comparison, in the PDI-based strong electron acceptors like (CN)₄(Cl)₄PDI, which forms ambient stable dianions, the ΔE was found to be 336 and 104 mV in CH₂Cl₂ and MeOH, respectively.^{12c}

The optical properties of **1** and **2a–d** were explored further by UV–vis absorption and emission spectroscopy and compared to those of **3** and **4** (Table S3A). With an increase in the number of bromine atoms in the perylenediimide core, both the absorption and the emission maxima undergo a gradual red-shift (Figure 4). Thus, **3**, **4**, **1**, and **2d** showed

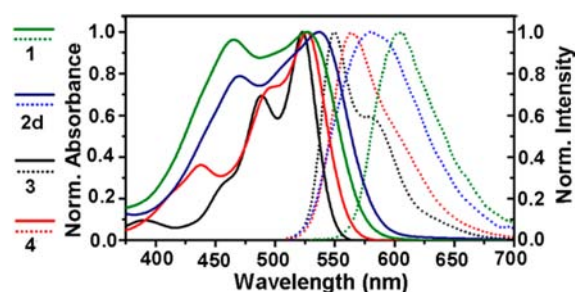


Figure 4. UV–vis (solid lines) and fluorescence (dotted lines) spectra of **1**, **2d**, **3**, and **4** in CH₂Cl₂, ($\lambda_{\text{ex}} \sim 500$ nm).

absorption maxima in dichloromethane solution at 522, 526, 527, and 535 nm, respectively, while the emission maxima were located at 549, 563, 603, and 580 nm, respectively. Notably, the emission spectra of **1** and **2d** underwent a red-shift of more than 30–50 nm compared to **3**. These results confirmed that multiple bromine atoms can drive stabilization of the π^* orbitals in the PDI scaffold resulting in the large-red shifts in the absorption and emission spectra. On the other hand, **5a–c** exhibit intense intramolecular charge-transfer absorption bands and weak emission (Table S3B).

Next, **2a** was found to undergo facile chemical reduction with mild reducing agents. A single-electron transfer (SET) reaction was realized upon gradual addition of TBACN to **2a** with the formation of the **2a \cdot^-** radical anion under ambient conditions (see the SI). ESR spectroscopy of the isolated solid confirmed the formation of **2a \cdot^-** with a $g = 2.004$ with a peak-to-peak width of 29.16 G (Figure S6). Furthermore, the formation of **2a \cdot^-** could be followed by ESI-MS (Figure S20) and UV–vis–NIR absorption spectroscopy due to its persistent stability in solution state. New sets of bands of **2a \cdot^-** due to the $D_0 \rightarrow D_n$ transitions appeared at 680, 792 (most intense), 937, and 1055 nm, with gradual weakening of the 465 and 534 nm bands of **2a** (Figure S7). In comparison, the bay-substituted bis-CF₃–PDI radical anion^{13a} shows absorption bands at 695, 776, and 842 nm, while the unsubstituted PDI radical anions absorb at 699, 761, and 794 nm.^{13b}

Finally, the semiconductor properties of **2a–c** and **2e** were evaluated in bottom-gate top-contact organic thin-film transistors (OTFTs) fabricated by vapor deposition (in vacuum, at $\sim 5 \times 10^{-6}$ Torr) on octadecyltrichlorosilane (OTS)-functionalized or poly(methyl methacrylate) (PMMA) (~ 30 nm thick)-coated n-doped Si(gate)/SiO₂ (300 nm thick, dielectric) substrates. The devices were completed by thermal evaporation of 50 nm thick Au top source/drain electrodes. Note that only **2a** exhibits a clean evaporation under high vacuum, whereas the other PDIs exhibit considerable decomposition, as seen by the optical images of the residue in the crucible (Figure S8). This is probably the result of the very large molecular mass of these systems. However, these molecules are n-channel semiconductors when measured in vacuum (Figure S9). Not surprisingly, the best electron mobilities (μ_e 's) were found for **2a**, which approach $\sim 2 \times 10^{-3}$ cm²/V·s, whereas the maximum μ_e 's of the other PDIs were found to be $\sim 10^{-4}$ cm²/V·s (Table S4). It is important to note that the reported μ_e 's for previously described bay position substituted Br₂–PDI and Br₄–PDI derivatives are $\sim 10^{-5}$ – 10^{-6} cm²/V·s.¹² The greater μ_e 's could be possibly rationalized by structural rigidification/close-packing due to the halogen-bonding interactions and reduced LUMO energy.

In conclusion, we realized octabromination of PDA and synthesized several Br₈-PDI derivatives and new donor–acceptor combinations. Extensive core bromination enables solubility in common organic solvents, which is unknown for a PDA scaffold. The emergent features include very low reduction potentials, red-shifted optical features, and formation of persistent radical anions. Furthermore, enhanced TFT electron transport was found compared to other bis-/tetrahalogenated PDIs. The diverse halogen-bonding established for the first time in the PDA/PDI systems should open up new crystal engineering prospects toward promising electronic materials.¹⁴

■ ASSOCIATED CONTENT

Supporting Information

The Supporting Information is available free of charge on the ACS Publications website at DOI: 10.1021/acs.orglett.5b03513.

synthesis and analytical characterization of the molecules by NMR, MALDI-TOF MS, TEM, and UV–vis spectroscopy; CV and DPV studies; theoretical studies (PDF)

X-ray data for **1** (CIF)

X-ray data for **2a** (CIF)

■ AUTHOR INFORMATION

Corresponding Authors

*E-mail: a-facchetti@northwestern.edu.

*E-mail: m_pritam@mail.jnu.ac.in.

Notes

The authors declare no competing financial interest.

■ ACKNOWLEDGMENTS

P.M. thanks DST, Government of India, for the Swarnajayanti Fellowship (DST/SJF-02/CSA-02/2013-14), DBT-BT/PR5006/INF/153/2012 for the EPR facility, and DST-FIST for funding the instrumentation facilities at CIF, SPS, JNU. A.F. thanks the US–Israel Binational Science Foundation (BSF, no. SP0022069). A.F. also thanks the Binational Science Foundation (BSF, No. 2012250) for support of this research. Y.K., S.K.K., and S.S.S. thank CSIR and S.K., J.S. thanks UGC for their research fellowships. P.M. thanks AIRF, JNU, New Delhi, for the other instrumentation facilities. We thank Dr. D. Das, SPS, JNU, for help with the X-ray data collection of **1**.

■ REFERENCES

- (1) (a) Huang, C.; Barlow, S.; Marder, S. R. *J. Org. Chem.* **2011**, *76*, 2386. (b) Görl, D.; Zhang, X.; Würthner, F. *Angew. Chem., Int. Ed.* **2012**, *51*, 6328. (c) Weil, T.; Vosch, T.; Hofkens, J.; Peneva, K.; Müllen, K. *Angew. Chem., Int. Ed.* **2010**, *49*, 9068. (d) Rademacher, A.; Markle, S.; Langhals, H. *Chem. Ber.* **1982**, *115*, 2927. (e) Demmig, S.; Langhals, H. *Chem. Ber.* **1988**, *121*, 225.
- (2) (a) Tsarfati, Y.; Strauss, V.; Kuhri, S.; Krieg, E.; Weissman, H.; Shimon, E.; Baram, J.; Guldi, D. M.; Rybtchinski, B. *J. Am. Chem. Soc.* **2015**, *137*, 7429. (b) Mattiello, S.; Sanzone, A.; Brazzo, P.; Sassi, M.; Beverina, L. *Eur. J. Org. Chem.* **2015**, *2015*, 5723. (c) Zhan, X.; Facchetti, A.; Barlow, S.; Marks, T. J.; Ratner, M. A.; Wasielewski, M. R.; Marder, S. R. *Adv. Mater.* **2011**, *23*, 268. (d) Sanguineti, A.; Sassi, M.; Turrissi, R.; Ruffo, R.; Vaccaro, G.; Meinardi, F.; Beverina, L. *Chem. Commun.* **2013**, *49*, 1618. (e) Sforazzini, G.; Orentas, E.; Bolag, A.; Sakai, N.; Matile, S. *J. Am. Chem. Soc.* **2013**, *135*, 12082.
- (f) Charbonnaz, P.; Zhao, Y.; Turdean, R.; Lascano, S.; Sakai, N.; Matile, S. *Chem. - Eur. J.* **2014**, *20*, 17143.
- (3) Watson, M. D.; Fechtenkötter, A.; Müllen, K. *Chem. Rev.* **2001**, *101*, 1267.
- (4) (a) Würthner, F.; Stepanenko, V.; Chen, Z.; Saha-Möller, C. R.; Kocher, N.; Stalke, D. *J. Org. Chem.* **2004**, *69*, 7933. (b) Qiu, W.; Chen, S.; Sun, X.; Liu, Y.; Zhu, D. *Org. Lett.* **2006**, *8*, 867. (c) Jiang, W.; Xiao, C.; Hao, L.; Wang, Z.; Ceymann, H.; Lambert, C.; Motta, S. D.; Negri, F. *Chem. - Eur. J.* **2012**, *18*, 6764.
- (5) Zagranyarski, Y.; Chen, L.; Jänsch, D.; Gessner, T.; Li, C.; Müllen, K. *Org. Lett.* **2014**, *16*, 2814.
- (6) Dubey, R. K.; Westerveld, N.; Grozema, F. C.; Sudhölter, E. J. R.; Jager, W. F. *Org. Lett.* **2015**, *17*, 1882.
- (7) (a) Sadrai, M.; Hadel, L.; Sauers, R. R.; Husain, S.; Krogh-Jespersen, K.; Westbrook, J. D.; Bird, G. R. *J. Phys. Chem.* **1992**, *96*, 7988. (b) Gsänger, M.; Oh, J. H.; Könemann, M.; Höffken, H. W.; Krause, A.-M.; Bao, Z.; Würthner, F. *Angew. Chem., Int. Ed.* **2010**, *49*, 740. (c) Yue, W.; Jiang, W.; Böckmann, M.; Doltsinis, N. L.; Wang, Z. *Chem. - Eur. J.* **2014**, *20*, 5209.
- (8) Konemann, M.; Mattern, G. WO2009/000831A1, 2008.
- (9) (a) Priimagi, A.; Cavallo, G.; Metrangolo, P.; Resnati, G. *Acc. Chem. Res.* **2013**, *46*, 2686. (b) Boterashvili, M.; Shirman, T.; Cohen, S. R.; Evmenenko, G.; Dutta, P.; Milko, P.; Leitun, G.; Lahav, M.; van der Boom, M. E. *Chem. Commun.* **2013**, *49*, 3531. (c) Mukherjee, Desiraju, G. R. *IUCr* **2014**, *1*, 49. (d) Desiraju, G. R.; Parthasarathy, R. *J. Am. Chem. Soc.* **1989**, *111*, 8725.
- (10) PDA and core-functionalized PDA have been known to be soluble only in DMSO, DMF, and strongly acidic medium.
- (11) CCDC (1430855) (**1**) and CCDC (1412900) (**2a**) contain the crystallographic data for this paper.
- (12) (a) Schmidt, R.; Oh, J. H.; Sun, Y.-S.; Deppisch, M.; Krause, A.-M.; Radacki, K.; Braunschweig, H.; Könemann, M.; Erk, P.; Bao, Z.; Würthner, F. *J. Am. Chem. Soc.* **2009**, *131*, 6215. (b) Jones, B. A.; Facchetti, A.; Wasielewski, M. R.; Marks, T. J. *J. Am. Chem. Soc.* **2007**, *129*, 15259. (c) Seifert, S.; Schmidt, D.; Würthner, F. *Chem. Sci.* **2015**, *6*, 1663.
- (13) (a) Roznyatovskiy, V. V.; Gardner, D. M.; Eaton, S. W.; Wasielewski, M. R. *Org. Lett.* **2014**, *16*, 696. (b) Ajayakumar, M. R.; Yadav, S.; Ghosh, S.; Mukhopadhyay, P. *Org. Lett.* **2010**, *12*, 2646.
- (14) (a) Meazza, L.; Foster, J. A.; Fücke, K.; Metrangolo, P.; Resnati, G.; Steed, J. W. *Nat. Chem.* **2012**, *5*, 42. (b) Voth, A. R.; Khuu, P.; Oishi, K.; Ho, P. S. *Nat. Chem.* **2009**, *1*, 74. (c) Shirman, T.; Freeman, D.; Posner, Y. D.; Feldman, I.; Facchetti, A.; van der Boom, M. E. *J. Am. Chem. Soc.* **2008**, *130*, 8162–8163. (d) Metrangolo, P.; Carcenac, Y.; Lahtinen, M.; Pilati, T.; Rissanen, K.; Vij, A.; Resnati, G. *Science* **2009**, *323*, 1461.